

Full length article

Anomalous transverse effects and Magneto-Optical properties of Co-based Heusler Compounds

Anusree C.V^a, Alexander N. Rudenko^b, M. Manivel Raja^c, V. Kanchana^{a,*}^a Department of Physics, Indian Institute of Technology Hyderabad, Kandi 502285, Sangareddy, Telangana, India^b Radboud University, Institute for Molecules and Materials, 6525AJ Nijmegen, The Netherlands^c Advanced Magnetic Group, Defence Metallurgical Research Laboratory, Kanchanbagh P.O- 500058, Hyderabad Telangana, India

ARTICLE INFO

Keywords:

Electronic structure
Magnetic interactions
Anomalous transverse effects
Magneto-optical Kerr effect

ABSTRACT

The interplay between magnetism and topology has brought new prospects in condensed matter physics and material science. By virtue of dissipation-free transport, a special band structure, and a greater Berry curvature, linear response in topological materials is greatly enhanced. The topological band structure in conjunction with symmetries plays a pivotal role in designing state-of-the-art materials with strong and exotic electromagnetic responses, providing favourable mechanisms for the upcoming generation of technological applications. The present work is mainly focused on an intuitive understanding of the anomalous transport coefficients and magneto-optical response in magnetic materials, particularly in regular Co-based Heusler compounds in the framework of the first-principles calculations. The ferromagnetic nature is probed through the Heisenberg exchange interactions and the Curie temperature (T_c) is estimated. With the inclusion of spin-orbit coupling in combination with non-collinear magnetization, the protective symmetries are broken consequently inducing non-vanishing valleys and peaks in the Berry curvature. The calculated values of intrinsic anomalous Hall conductivity (AHC) are 462 S/cm, 371 S/cm and 374 S/cm for the Co_2HfZ ($Z = \text{Sn}$, Al , and Ga) and corresponding values of anomalous Nernst conductivity (ANC) are 5.6 A/m/K, -2.3 A/m/K, and 3.7 A/m/K respectively. Additionally, the magneto-optical response is also studied and the corresponding polar Kerr rotation angles at normal incidence were found to be 1.2° for Co_2HfSn , 1.1° for Co_2HfAl and 0.8° for Co_2HfGa . Hence, this study may pave the way to scrupulous engineering of the material properties to realize the technologically desirable applications.

1. Introduction

The evolution of the past decade with the advancement of sophisticated and innovative materials with exotic features has enhanced the demand for potential technological applications. One such avenue in present condensed matter research which revolutionized the present information technology is spintronics or spin transport electronics [1–3]. Lord Kelvin's discovery of anisotropic magnetoresistance (AMR) 107 years ago made the way for spin electronics [4], and the realm of spintronics path to practical applications was facilitated with the astounding discovery of gigantic magnetoresistance [5,6]. A very noted application of spintronics can be seen in the development of magnetic random-access memory (MRAM) [7,8]. In the initial stage, MRAMs were using the GMR effect with the storage capacity being 4 MB. With the advent of tunnelling magnetoresistance (TMR) [9,10] and spin-transfer torque (STT) [11], the capacity has increased to 256 MB [7]. This became possible by exploiting the spin degrees of freedom of the electron along with its charge, thereby giving rise to a new class of

material called spintronic materials. Like any upcoming techniques, the challenges in the field of spintronics make this more interesting research field, and one of the challenges is the achievement of 100% spin polarization or pure spin current [12], and it must be recognized that the maximal spin polarization achieved in practise is less than 50% [13], emphasizing the need for more research. Research for an efficient spintronic material for practical application which can provide 100% spin polarization and which is functional at room temperature will be worthwhile.

Topological phases of matter are well known for their extrinsic properties which can be explored under the lens of a branch of mathematics, concerned with the invariant geometry of objects under smooth deformations called topology in conjunction with spins of magnetic materials. Extracting the novel and environment-friendly materials with desired properties such as ultralow energy consumption in order to meet the energy requirements and high-speed technology to withstand

* Corresponding author.

E-mail address: kanchana@phy.iith.ac.in (V. Kanchana).

the present information technology is a highly demanding process. Quantum emergence set the ground for these growing technological developments. Quantum materials provide a firm basis in major fields of research which include magnetism, superconductivity, thermoelectrics, photovoltaics, quantum computing and communications, etc. [12,14–17]. Materials with electronic or magnetic structures hosting exotic knots or twists which require a change in their fundamental nature for untangling are referred to as topological or topologically non-trivial. Such non-trivial topologies have been found in a new class of quantum materials among insulators and semi-metals. The wide range of characteristics exhibited by these materials include the fermionic excitations like Weyl, Dirac, or Majorana, topological surface states, and non-collinear spin textures such as skyrmions. Most of these properties arise from the elementary symmetries of the bulk crystal and a common feature among these properties is the topologically protected direct connection to non-equilibrium phenomena with a huge response towards the external stimuli. Thus far, non-magnetic topological materials have been found to possess exotic transport behaviours and topological phases, for example, topological insulators have topological surface states [18,19], Dirac semimetals have ultra-high carrier mobility, huge electrical and thermal magnetoresistance, and Weyl semimetals have large Nernst effect [20–23], chiral anomaly, and negative magnetoresistance [24,25].

A remarkable class of intermetallic materials with extremely flexible electronic structures are the Heusler compounds [26–29], which can be grown in thin films [30–33] and have high T_c [34]. Magnetism in conjunction with topological features make Heusler compounds a promising candidate for the exploration of the intrinsic Berry curvature (BC) [35–38] induced linear response effects like anomalous Hall effect (AHE) [39,40], anomalous Nernst effect (ANE) [41,42] and the magneto-optic Kerr effect (MOKE) [43–45]. The highest values of AHE reported in the ferromagnetic Weyl semimetals: $\text{Co}_3\text{Sn}_2\text{S}_2$, a Kagome crystal, and Co_2MnGa , a Heusler compound are more than 1000 S/cm [46,47]. Also, the maximum values of ANE reported for $\text{Co}_3\text{Sn}_2\text{S}_2$ [48] and Co_2MnGa [49] are 3 A/m/K and 7 A/m/K. Besides this, another interesting property hosted by Heusler alloys is the magneto-optical response which came into the limelight with the remarkable revelation of a colossal value of Kerr rotation angle for PtMnSb , which is greater than 2.0° at room temperature and 5° at 80 K which enhances the technological advancement in the magneto-optical field [50,51]. Hence, materials with a strong linear response effects have opened up the avenue for a wide range of technological applications that could be implemented in power electronics and thermoelectrics [16,17].

The present work is aimed to probe into the structural, magnetic and electronic properties of Co-based regular Heusler compounds Co_2HfZ ($Z = \text{Sn, Al and Ga}$) (Sections 3.1 and 3.2). The ferromagnetic ground state has been confirmed through Heisenberg exchange interactions and the Curie temperature estimation. Furthermore, to explore the anomalous linear response transverse effects, Berry curvature induced intrinsic AHC and ANC have been calculated (Section 3.3). Beyond this, magneto-optical aspects have also been analyzed (Section 3.4). A brief summary of our results is given in the last section (Section 4).

2. Computational details

Ab initio calculations were carried out for the present cubic Heusler systems using the pseudopotential projector augmented wave (PAW) [52] method implemented in the Vienna *ab initio* simulation package (VASP) [53]. A Plane-wave basis set with a kinetic energy cutoff of 700 eV was used. Generalized gradient approximation (GGA) with the Perdew–Burke–Ernzerhof (PBE) [54] exchange–correlation functional was used. The Γ -centred k-point mesh of $(16 \times 16 \times 16)$ was used for the Brillouin zone sampling. The ground-state energy configuration was attained with a maximum of 10^{-2} eV/Å force tolerance on each atom, where the lattice and atomic positions were

Table 1

Experimental and optimized lattice constants in Å and total magnetic moment per formula unit and per cobalt atom in Bohr magneton (μ_B).

Compound	a (exp)	a (opt)	m^{tot} (exp)	m^{tot} (opt)	m/Co
Co_2HfSn	6.227 [69]	6.26	1.55 [69]	2.000	1.066
Co_2HfAl	6.045 [70]	6.03	0.82 [70]	0.999	0.590
Co_2HfGa	6.032 [70]	6.03	0.60 [70]	1.005	0.584

optimized. The self-consistent charge density was determined using the total energy tolerance up to 10^{-6} eV/Å. The spin-polarized relativistic Korringa–Kohn–Rostoker (SPR-KKR) package [55] with $\text{l}_{max}=3$ for full potential spin-polarized scalar relativistic Hamiltonian with a k-mesh of $35 \times 35 \times 35$ for Brillouin Zone integration was used to estimate the Curie temperature (T_c) using mean-field approximation through Heisenberg magnetic exchange interactions. The maximally localized Wannier functions (MLWF) [56,57] were extracted via the WANNIER90 package [58] to generate the tight-binding Hamiltonian to calculate the BC through Kubo formalism [35,38,59]. The Anomalous transverse conductivity, AHC have been simulated using the WANNIERTOOLS package [60]. The MOKE calculations were performed using the BERRY module [61,62] of the WANNIER90 package.

3. Results and discussions

3.1. Structural and magnetic properties

The regular Heusler compounds Co_2HfZ ($Z = \text{Sn, Al and Ga}$) has been investigated in the fully ordered L21 structure which takes a cubic face-centred Bravais lattice with the space group $Fm\bar{3}m$ (No. 225), which stipulates the presence of several mirror symmetries. The crystal structure is shown in Fig. 1(a) with the atomic positions (1/4, 1/4, 1/4) for Co, (1/2, 1/2, 1/2) for Hf, and (0, 0, 0) for Z, with the magnetic moment alignment of cobalt atoms along the (001) direction. The crystal structure geometry was well-optimized by considering the available experimental lattice parameters as shown in Table 1. The total magnetic moment per f.u. of the compounds are $2 \mu_B$ for Co_2HfSn , $1 \mu_B$ for Co_2HfAl and Co_2HfGa which follows the Slater–Pauling [63] behaviour as given by

$$M = N_v - 24 \quad (1)$$

where N_v and M and are the total number of valence electrons and total magnetic moment in μ_B per f.u., respectively. Co_2HfSn , Co_2HfAl and Co_2HfGa have N_v of 26, 25 and 25 which further indicates the half-metallicity with integer values of M . From Table 1, it is found that these compounds are having a saturation magnetic moment of 1.55 μ_B , 0.82 μ_B and 0.60 μ_B experimentally per f.u. for Co_2HfZ ($Z = \text{Sn, Al, and Ga}$). B2-type disorder in Heusler alloys is evidenced [64–68] which may sometimes reduce the half-metallicity and be the reason for the reduced moment in experimentally prepared samples. These compounds show ferromagnetic behaviour with the magnetic moments aligned along (001) direction with the Curie temperatures as 394 K, 193 K, 186 K for Co_2HfSn [69], Co_2HfAl [70], and Co_2HfGa [70], respectively. The ferromagnetic nature of these compounds is due to the d -orbital interactions between the cobalt atoms. Through the crystal field symmetry, the splitting of the d orbitals into e_g and t_{2g} is schematically shown in Fig. 1(b). As the Co sites are in high spin states for the investigated Heusler compounds, the values of the local moment and e_g filling are obtained correspondingly as shown in Fig. 1(c).

From the spin-resolved density of states without spin-orbit coupling (SOC) shown in Fig. 4(a–c), it is seen that at the Fermi level one channel (down-spin) is fully gapped and the other one is metallic (up-spin) which demonstrates the half-metallic ground state of Co_2HfZ compounds, reconcilable with the existing experimental [69–71] and theoretical [72,73] studies. The compounds with 100% spin polarization is preferred for spintronic applications. The spin polarization of a

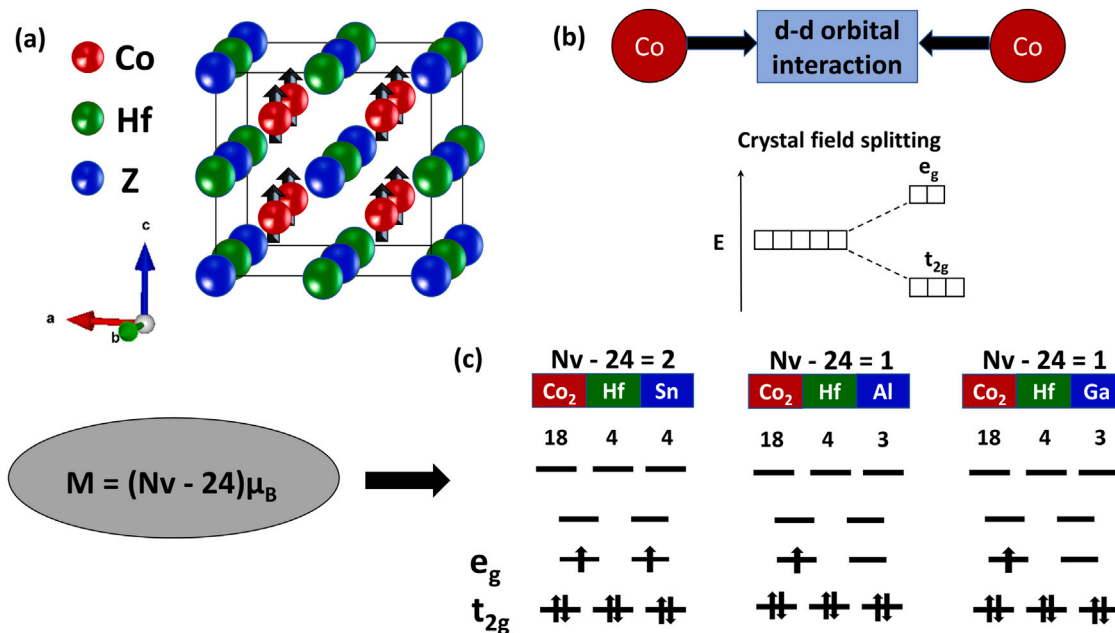


Fig. 1. (a) Crystal structure of Co_2HfZ ($Z=\text{Sn}, \text{Al}$ and Ga) with magnetic moment of cobalt atoms aligned along the (001) direction. (b) The d -orbitals interaction along with crystal field splitting of cobalt atoms. (c) The magnetic moment and electron occupation in the present series.

material can be found by knowing the contribution from up-spin and down-spin at the Fermi level. This can be found out by the equation:

$$P\% = \frac{N \uparrow (E_F) - N \downarrow (E_F)}{N \uparrow (E_F) + N \downarrow (E_F)} \times 100 \quad (2)$$

where $N \uparrow$ and $N \downarrow$ refer to the density of states contribution from the majority and minority spin channel. The Co_2HfZ series is found to be 100% spin-polarized as there is no contribution from the down-spin channel which indicates the profound spintronic applications.

The magnetic interactions were computed within the Heisenberg model for all the compounds using Munich spin-polarized relativistic Korringa–Kohn–Rostoker (SPRKRR) package [55]. The ground state magnetic configuration has been investigated based on the strength of interactions between the atoms in these compounds using the Heisenberg exchange coupling J_{ij} . The nature of magnetism exhibited by a system can be indicated by the exchange coupling constants. The J_{ij} values being positive and negative represents the ferromagnetic and anti-ferromagnetic coupling. The classical Heisenberg Hamiltonian allows one to estimate the exchange coupling amid the atoms by:

$$H_{eff} = - \sum_{\mu\nu} \sum_{ij} J_{ij}^{\mu\nu} e_i^\mu e_j^\nu \quad (3)$$

where i and j denotes the lattice vectors of the atoms within the sub-lattices, J_{ij} gives the exchange interactions between the i and j atomic sites and e_i^μ , e_j^ν specifies the unit vector pointing in the direction of magnetic moments along with the i and j atoms in discrete sublattices μ and ν , respectively. We have employed real-space Green's function approach in order to calculate magnetic exchange coupling, which is based on infinitesimal rotations of magnetic moments known as the Lichtenstein's formula [74] as implemented in the SPRKRR package. The estimation of Curie temperature (T_c) is done within the mean-field approximation [75] by:

$$T_C = \frac{2}{3k_B} J_{max} \quad (4)$$

With J_{max} being the largest eigen value of the effective exchange coupling matrix and J_{eff} is given by

$$J_{eff}^{\mu\nu} = \sum_{j \neq 0} J_{0j}^{\mu\nu} \quad (5)$$

Table 2
Experimental and estimated T_c in K.

Compound	T_c (exp)	T_c (MFA)
Co_2HfSn	394 [69]	593
Co_2HfAl	193 [70]	264.6
Co_2HfGa	186 [70]	246

with 0 and j referring to a specified and all atomic sites in the sub-lattice μ and ν within a sphere of radius $4.5a$ with a being the relaxed lattice constant of the compounds.

From Fig. 2(a) depicting the main magnetic coupling paths, it is found that the first nearest neighbour interactions in discrete sublattice and within the sublattice are given by J_1 and J'_1 . Whereas the second nearest neighbour interactions in discrete sublattice is given by J_2 . Hence, in the $\text{Co}_1\text{-Co}_2$ interactions, J is calculated between the atoms in the different sublattice, and in the $\text{Co}_1\text{-Co}_1/\text{Co}_2\text{-Co}_2$ interactions, J is calculated between the atoms in the same sublattice. The Heisenberg exchange coupling constant is plotted against R_{ij}/a , with R_{ij} and a being the nearest-neighbour distance and optimized lattice constant of the compounds studied, as depicted in Fig. 2(b, c and d). In all three compounds, the $\text{Co}_1\text{-Co}_2$ and $\text{Co}_1\text{-Co}_1/\text{Co}_2\text{-Co}_2$ interactions contribute more to the exchange coupling constant. As other interactions are quite negligible, they are omitted.

For Co_2HfSn , from Fig. 2(b) it is observed that the first four nearest-neighbour interactions are positive, whereas the next three are negative for $\text{Co}_1\text{-Co}_2$ and first two nearest-neighbour interactions are negative while the fourth, fifth and sixth are positive for $\text{Co}_1\text{-Co}_1/\text{Co}_2\text{-Co}_2$. This oscillating behaviour depicts the RKKY type of interactions. As the strength of the positive interactions dominate, the compound is found to be ferromagnetic in nature. Looking at the case of Co_2HfAl and Co_2HfGa from Fig. 2(c and d), it is found that for $\text{Co}_1\text{-Co}_2$, the first interaction is positive, the next three are negative, and the fifth is again positive, whereas for $\text{Co}_1\text{-Co}_1/\text{Co}_2\text{-Co}_2$ the first interaction is negative, the second one is positive, and the next four are negative.

As a result, the RKKY interactions reveal the ferromagnetic nature of the compounds. Table 2 shows that the estimated Curie temperature values derived from mean-field approximation [76] are higher than the experimentally reported values [77] which is not surprising because

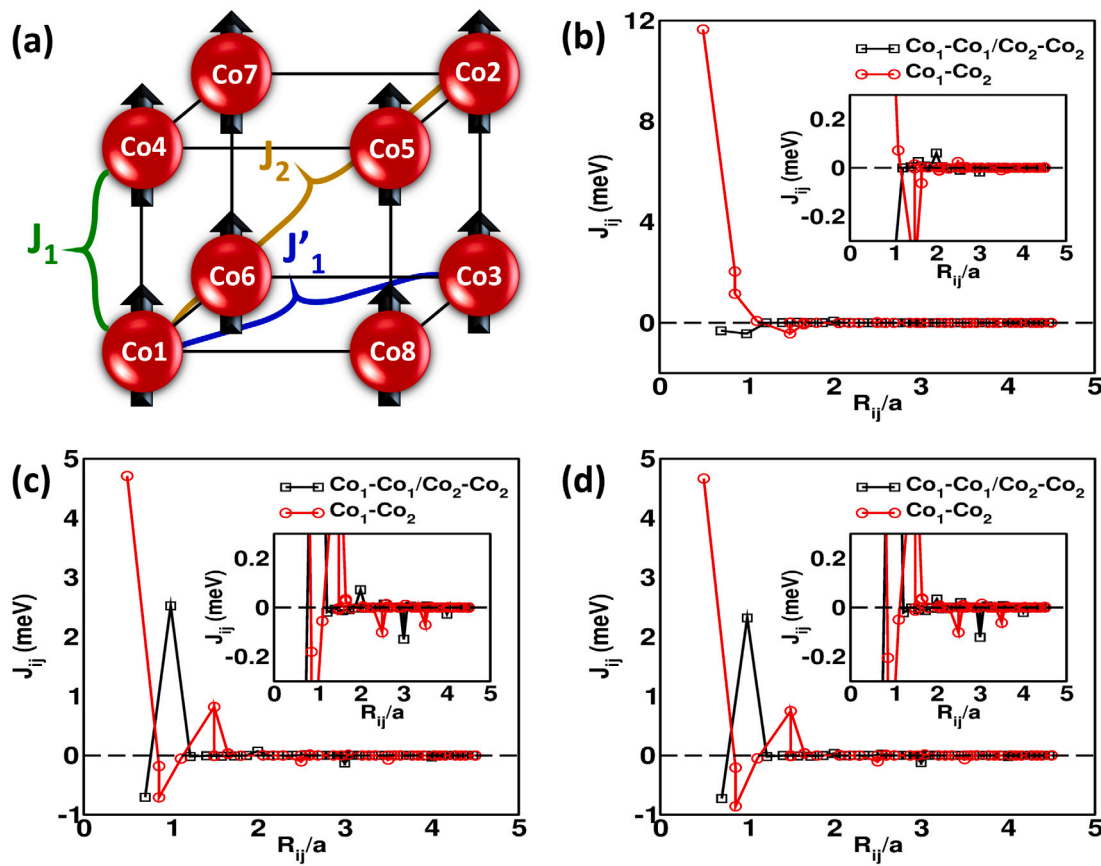


Fig. 2. (a) Visualization of main magnetic couplings. Heisenberg exchange interactions for Co_2HfSn in (b), Co_2HfAl in (c) and Co_2HfGa in (d) depicting the exchange coupling between $\text{Co}_1\text{-Co}_2$ and $\text{Co}_1\text{-Co}_1/\text{Co}_2\text{-Co}_2$.

it neglects magnetic fluctuations at long wavelengths. Another reason could be related to the role of ligands, whose spin polarization is not explicitly considered within the Heisenberg Hamiltonian Eq.(3) [78].

3.2. Electronic properties

It is known that magnetic Heusler compounds possess intriguing properties due to their band structure, which makes them a promising class of materials. From Fig. 3, it is found that the crystal structure without magnetization has three mirror planes at $k_x = 0$, $k_y = 0$, and $k_z = 0$. The magnetization along (001) direction with the inclusion of SOC breaks the mirror symmetries in the $k_x = 0$ and $k_y = 0$ plane. The change in the magnetization orientation breaks the symmetries differently. Only M_z mirror symmetry and C_{4z} rotational symmetry gets preserved in these compounds.

Looking at the Fermi surface of Co_2HfSn obtained without SOC from Fig. 3(a), two different pockets at the high symmetry point X are found which corresponds to two different bands crossing the E_F along Γ -X and U-K with the path $\Gamma\text{-X}\text{-U}\text{-K}\text{-}\Gamma\text{-L}\text{-W}\text{-X}$. As these two bands cross the E_F twice from valence band to conduction band and vice-versa, a closed contour nature is obtained. In the case of Co_2HfAl and Co_2HfGa from Fig. 3(b and c), a similar trend is seen as the hole and electron pockets correspond to two different bands crossing the E_F along W- Γ , $\Gamma\text{-X}$ and X-K with the path W-L- Γ -X-W-K. The two Fermi surfaces corresponds to two bands crossing the Fermi level in all the three compounds in Fig. 3.

The band structure of Co_2HfZ with $Z = \text{Sn}, \text{Al}$ and Ga with the inclusion of SOC along the path W-L- Γ -X-W-K are shown in Fig. 4(d-e). The major contribution comes from Co-d orbitals near the Fermi level compared to the other atomic orbitals. A closer introspection of band structure shows SOC induced gaps, which drives BC in the band

structure and resulting in the linear response transverse effects like AHE and ANE. This will be discussed in detail in Section 3.3.

3.3. Anomalous transverse effects

Mirror symmetries concurrent with magnetism play an important role in strong anomalous transverse effects. In ferromagnetic materials an additional transverse voltage get generated in response to the SOC effect, deflecting the charge carriers by the magnetic moment of the solid. This is recognized as the AHE [39,40]. An assessment of a material's topological phase can be made by its band structure property, such as the BC [35-38]. It is possible to generate a non-zero AHE and a finite net BC in the absence of symmetry operations that reverse the sign of the local Berry curvature in the Brillouin zone, when reversing the sign of the momentum vector: mirror operations and time-reversal symmetry operations. As far as BC and AHE are concerned, the control is gained through the manipulation of symmetries and band structures independent of finite magnetization values.

In amalgamation with SOC, magnetization direction determines the manner in which symmetry of the system is broken, resulting in a large BC being induced near the Fermi energy. The AHE is characterized by unvanishing valleys and peaks in the Berry curvature when SOC is included and ANE is caused by the generation of transverse electric voltage perpendicular to both magnetization and an applied thermal gradient [41,42]. It is also known as the thermoelectric counterpart of AHE and can generate a strong Nernst thermopower under a low magnetic field. Berry curvature, or non-trivial geometry of the wavefunction of electrons, drives the ANE, which is proportional to the material's magnetization. The Berry curvature of the occupied bands near the Fermi level leads to AHE and ANE. The Berry curvature is zero in the absence of anti-crossings, which usually takes place when

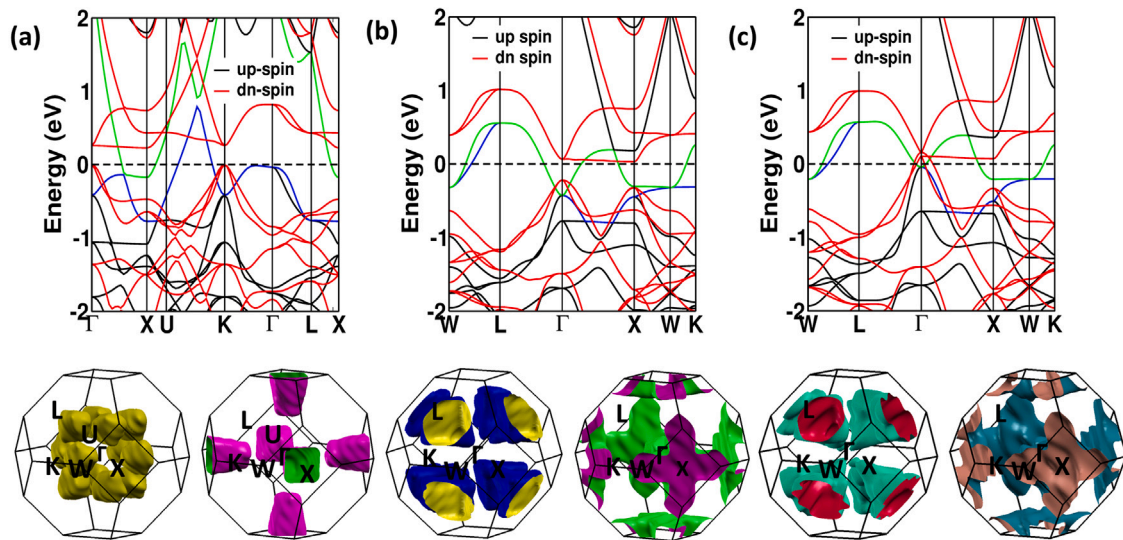


Fig. 3. (a–c) The Fermi Surface topology with corresponding band structure of Co_2HfSn , Co_2HfAl and Co_2HfGa without SOC. The bands crossing the E_F which corresponds to two Fermi Surface are shown by green and blue lines.

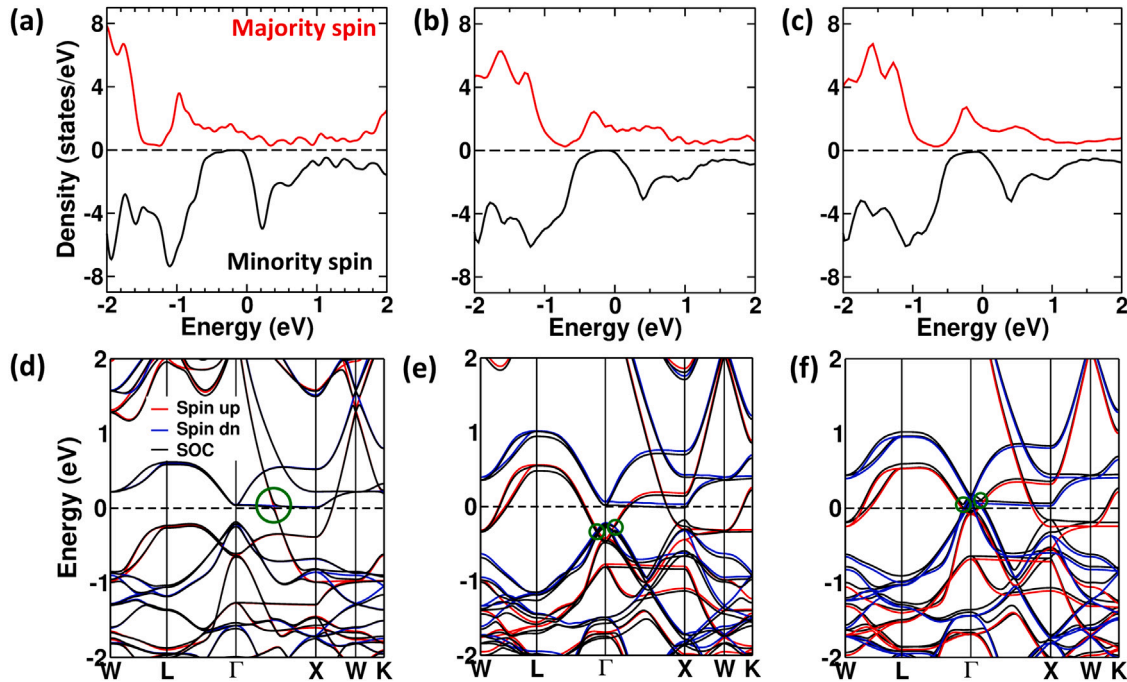


Fig. 4. (a–c) The spin-resolved density of states without SOC. (b–d) The band structure of Co_2HfZ with $Z = \text{Sn}$, Al and Ga with and without the inclusion of SOC.

bands of opposite spin cross in presence of SOC. An illustration of the onset of transverse effects from the band structure has been pretty well described schematically without making reference to the spin in Fig. 5.

We now discuss our scheme for calculating the Berry curvature, AHC and ANC. As the magnetization orientation of the present series is along the z -direction, only the z component Ω_n^z is not equal to zero. From the maximally localized Wannier functions obtained, a tight-binding Hamiltonian, H is constructed to calculate the BC, Ω_n^z through the Kubo-formula [62].

$$\Omega_n^z(\mathbf{k}) = -2\text{Im} \sum_{m \neq n} \frac{\langle \psi_{nk} | v_x | \psi_{mk} \rangle \langle \psi_{mk} | v_y | \psi_{nk} \rangle}{[E_m(\mathbf{k}) - E_n(\mathbf{k})]^2}, \quad (6)$$

where n is the index of the occupied bands, \mathbf{k} is the wave vector, $E_n(\mathbf{k})$ is the eigenvalue of n th eigenstate ψ_{nk} , v 's are the velocity operators.

AHC is extracted from Berry curvature with the principle transport parameter σ_{xy} via

$$\sigma_{xy} = -\frac{e^2}{\hbar} \int_{BZ} \frac{d^3k}{(2\pi)^3} \sum_n f(k) \Omega_n^z(k), \quad (7)$$

and $f(k)$ is the Fermi-Dirac distribution function. ANC, α_{xy} as proposed by Xiao et al. [36,38]

$$\alpha_{xy}(T, \mu) = -\frac{1}{e} \sum_n \int d\epsilon \frac{\partial f(\epsilon - \mu, T)}{\partial \epsilon} \cdot \frac{\epsilon - \mu}{T} \sigma_{xy}(\epsilon), \quad (8)$$

where T is the temperature, μ is the chemical potential. As T tends to zero, the equation gets modified as

$$\left. \frac{\alpha_{xy}}{T} \right|_{T \rightarrow 0} = -\frac{\pi^2}{3} \frac{k_B^2}{|e|} \frac{d\sigma_{xy}}{d\mu} \quad (9)$$

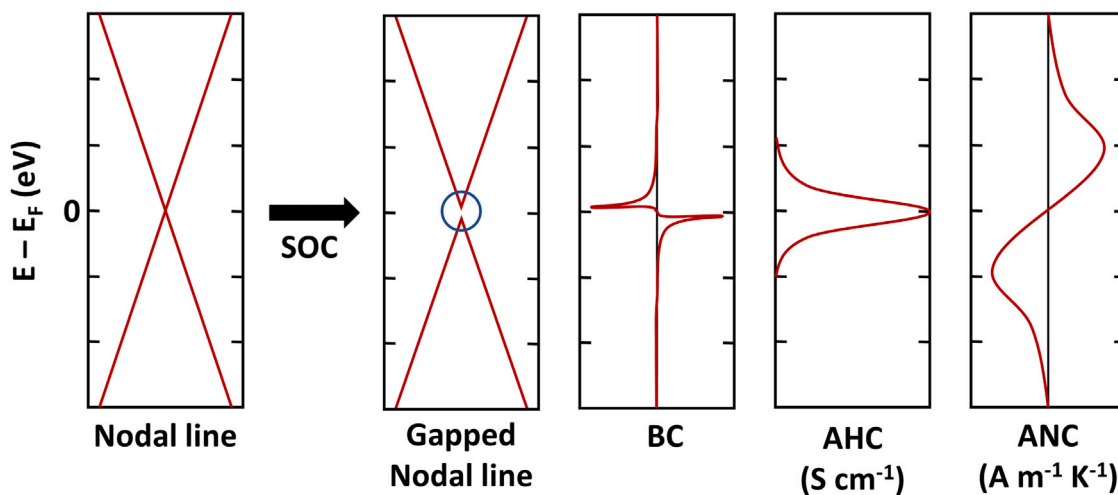


Fig. 5. Illustration of onset of transverse effects A model showing the band structure of a system without and with SOC, inducing BC and leading to AHE and ANE.

Table 3

Calculated maximum values of AHC in S/cm and ANC in A/m/K at 300 K with their corresponding energy within the range of ± 300 meV around the Fermi level E_F .

Compound	AHC	Energy	ANC	Energy
Co ₂ HfSn	462	-255	5.6	-226.8
Co ₂ HfAl	371	-206.4	-2.3	-250
Co ₂ HfGa	374	-35.2	3.7	-0.6

In the present series, from the band structure with SOC as given in Fig. 4(d–f) avoided crossings are found, which induces BC and consequently leads to AHE and ANE. In Fig. 6(a, b and c), the induced BC in the band structure along with AHC and ANC peaks obtained for the three compounds are shown. Generally, the AHC peaks occur at the energy level where band crossings or nodal lines occur. Interestingly, in this series, the peaks are not found where crossings open up with the inclusion of SOC. Similar behaviour is found in a few other materials [15,79]. The lack of a large density of states near the Fermi level could be a probable reason, which can eventually provide a diminishing effect on both BC and AHC [80]. The same nature is observed in the present series as seen from Fig. 6(a, b and c) for Co₂HfSn, Co₂HfAl and Co₂HfGa. The net magnitude of AHC in weak SOC systems is also influenced by the percentage of spin polarization.

In our proposed series, a 100% spin polarization is observed at the Fermi level which suppresses the AHC values and the mixture of spin up and down states enhances the AHC values. The calculated maximum values of AHC and ANC with their corresponding energy levels extracted within a range of ± 300 meV around the Fermi level at 300 K is given in Table 3, which is found to be comparable with the values of other Heusler compounds reported in the literature [81–83].

3.4. Magneto-optical Kerr effect (MOKE)

The past decades have witnessed the magneto-optical properties in ferromagnetic materials gaining wider attention. The magneto-optical Kerr effect (MOKE) is observed when a linearly polarized electromagnetic wave is incident on the surface of a magnetic material, where the polarization of the reflected wave undergoes a change and becomes elliptic [84]. MOKE has been exploited in recent years in probing a broad range of layered magnetic systems, thin magnetic films, and magnetic superlattices [85–87]. MOKE has also been used to study the behaviour of nanomagnets arranged in the linear chain [88]. The velocity of large domain walls in ultrathin magnetic nanowires has been measured by MOKE [89] and the magnetization response of individual macromolecules has been studied using MOKE microscopy up to

200 nm in spatial resolution [90]. The reciprocity between the SOC and exchange interactions during interband transitions between the occupied and the unoccupied valence states is the physical mechanism responsible for MOKE [91]. As a result of which the polarization plane of the reflected wave gets rotated with concerning the incident wave forming a rotation angle called Kerr angle. The extent of rotation (or the magnitude of the Kerr angle) depends on several factors like the direction of the wave vector of the incident wave, the magnetization orientation of the material, and the geometry of the surface from which the wave gets reflected. Since we consider cubic Heusler systems with magnetization along the z-axis, the polar Kerr effect could be observed. The optical conductivity tensor can be written as:

$$\sigma = \begin{pmatrix} \sigma_{xx} & \sigma_{xy} & 0 \\ -\sigma_{xy} & \sigma_{xx} & 0 \\ 0 & 0 & \sigma_{zz} \end{pmatrix}$$

The macroscopic conductivity tensor $\sigma_{xy}(\hbar\omega)$ is taken into account to form the complex polar Kerr angle (ϕ_K), as shown in [58]:

$$\sigma_{xy}(\hbar\omega) = \frac{ie^2\hbar}{N_k\Omega_c} \sum_k \sum_{n,m} \frac{f_{mk} - f_{nk}}{\epsilon_{mk} - \epsilon_{nk}} \frac{\langle \psi_{nk} | v_x | \psi_{mk} \rangle \langle \psi_{mk} | v_y | \psi_{nk} \rangle}{\epsilon_{mk} - \epsilon_{nk} - (\hbar\omega + i\eta)}, \quad (10)$$

where $\hbar\omega$ is the optical frequency, N_k is the number of k-points used for Brillouin zone sampling and Ω_c is the cell volume and η will have an infinitesimal positive value. In the limit of large material thickness, the Kerr angle θ_K for normal incidence is calculated using the polar MOKE equation [92]

$$\phi_K = \theta_K + i\gamma_K = \frac{-\sigma_{xy}}{\sigma_{xx}\sqrt{1 + i(\frac{4\pi}{\omega})\sigma_{xx}}}, \quad (11)$$

where θ_K is the real Kerr-rotation angle, γ_K is the Kerr ellipticity and σ_{xx} , σ_{xy} are the optical conductivity tensor components. The Kubo formula connects the macroscopic conductivity tensor components with the microscopic optical transitions. When electromagnetic radiation strikes these compounds, the magnetic component of light interacts with their magnetic moments. Therefore, the polarized light is visible as a result of the reflection of photons from their surfaces as depicted schematically in Fig. 7(a).

In the case of Co₂HfSn, it is observed from Fig. 7(b) that the Kerr angle (θ_K) varies with positive and negative peaks indicating a clockwise and counterclockwise polarization direction which confirms polarization has occurred in the light. On either side of the visible region, both negative and positive peaks are found indicating a Kerr rotation angle of -0.7° and $+1.2^\circ$. In the visible region, a negative peak is observed with a value of -0.6° . As well, other positive and negative peaks are observed away from the visible region, which indicates that

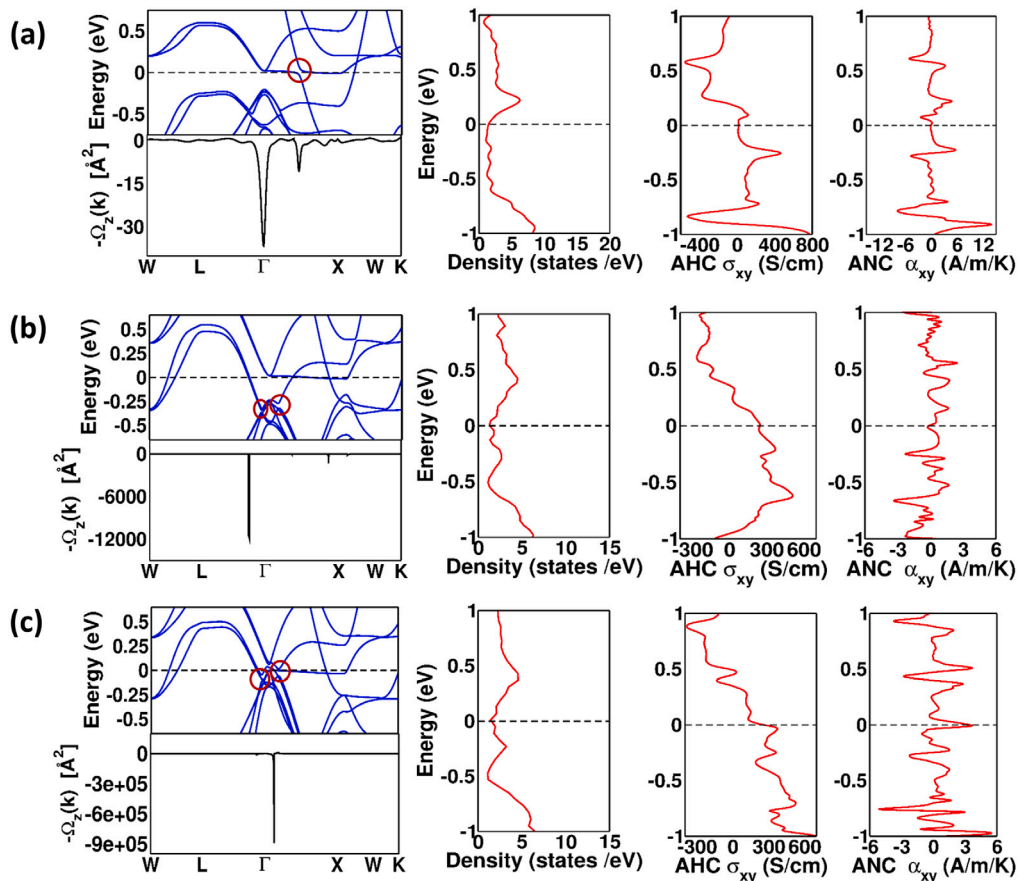


Fig. 6. Berry curvature $\Omega_z(k)$ along high symmetry path, density of states with the inclusion of SOC, anomalous Hall conductivity (σ_{xy}) and anomalous Nernst conductivity (α_{xy}) calculated within the range of ± 300 meV around Fermi level at 300 K for Co₂HfSn, Co₂HfAl and Co₂HfGa in (a), (b) and (c).

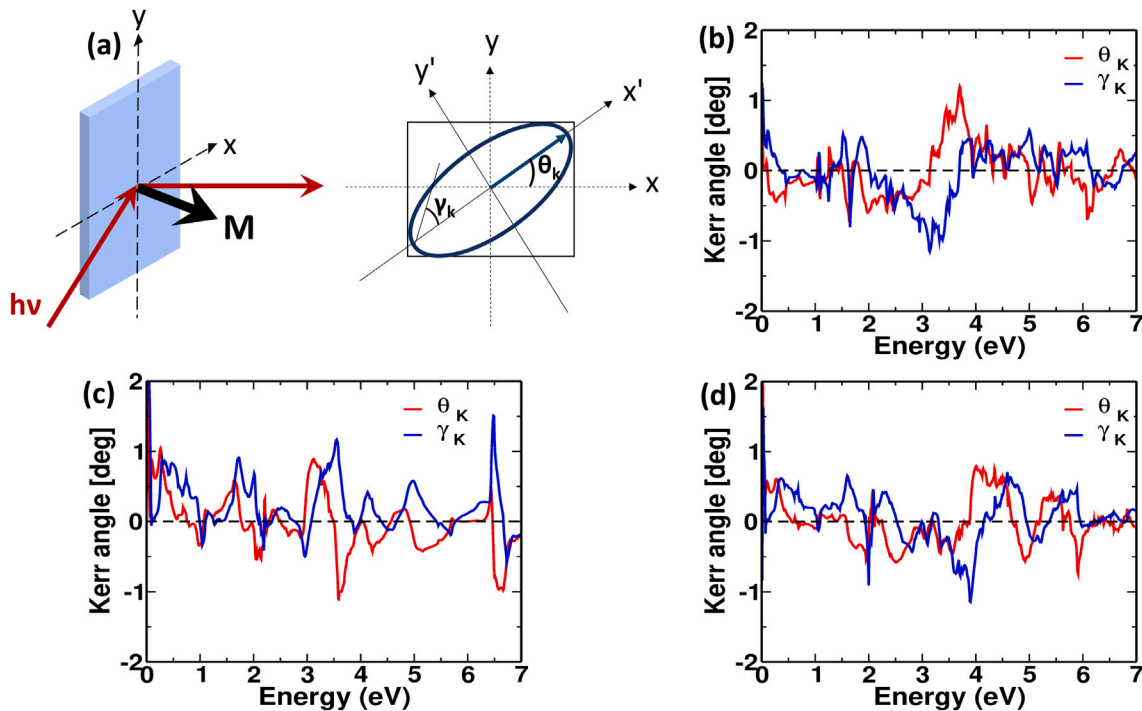


Fig. 7. (a) Depiction of the polar Kerr effect. The Kerr angle (θ_K) and ellipticity (γ_K) calculated at normal incidence versus optical energy for Co₂HfSn (b), Co₂HfAl (c), and Co₂HfGa (d).

Compound	$\theta_K(max)$
Co ₂ HfSn	1.2
Co ₂ HfAl	1.1
Co ₂ HfGa	0.8

varying the energy of the reflected photon will affect the rotation of the electric field of reflected light in both a clockwise and counterclockwise direction. Hence, we observe a change of both polarization and magnitude.

Considering the case of Co₂HfAl from Fig. 7(c), it is found that θ_K is having negative peaks of values -0.3° , -0.5° , and -1.1° and positive peaks of 0.5° and 0.8° in the energy range of 1 to 4 eV. Hence, the rotation and polarization of the electric field are more in the anticlockwise direction, which is confirmed by the peak values of γ_K corresponding to the rotation.

Looking at Co₂HfGa from Fig. 7(d), it observed that between 1 to 6 eV considerable negative peaks are found with θ_K values of -0.5° , -0.6° and -0.7° a positive peak of value 0.8° at 4 eV. Therefore, it is noticed that the electric field rotation is from counterclockwise to clockwise as well as its polarization.

Hence, we conclude that a similar trend is depicted in all three compounds of this series. The polar Kerr angle at normal incidence is found to be comparable to the values of the other Heusler compounds in the literature [82]. The maximal value of Kerr angle is taken in a range from 1 to 5 eV and given in Table 4.

4. Conclusion

In summary, a systematic investigation of the structural, magnetic and electronic properties of the regular Heusler Co-based compounds is done using the first principle studies. From the initial analysis of the above mentioned features, the present series is found to be half-metallic in nature and the ground state ferromagnetic configuration is found out via the Heisenberg exchange interactions with the T_c estimation. A close inspection of the electronic band structure with magnetism in conjunction with topology lead us to look into the anomalous transverse effects. The non-vanishing valleys and peaks of the Berry curvature with the inclusion of the SOC resulted in the intrinsic contribution of the anomalous Hall conductivity values of 462 S/cm, 371 S/cm and 374 S/cm for the Co₂HfZ (Z= Sn, Al and Ga) and corresponding anomalous Nernst conductivity values as 5.6 A/m/K, -2.3 A/m/K and 3.7 A/m/K. Furthermore, the magneto-optical response has been studied and the polar Kerr rotation angles of 1.2° for Co₂HfSn, 1.1° Co₂HfAl and 0.8° for Co₂HfGa are obtained at normal incidence. From the above discussion, it is evident that the Co₂HfZ series is indeed a promising candidate for future spintronic applications. If the Fermi level's position can be tuned through doping or external strain/pressure without compromising the band profile then this series could also be advantageous for the field of topological materials.

CRediT authorship contribution statement

Anusree C.V: Software, Methodology, Validation, Visualization, Writing – review & editing. **Alexander N. Rudenko:** Methodology, Validation, Writing – review & editing. **M. Manivel Raja:** Validation, Writing – review & editing. **V. Kanchana:** Conceptualization, Software, Methodology, Validation, Visualization, Project administration, Writing – review & editing.

Declaration of competing interest

The authors declare that they have no known competing financial interests or personal relationships that could have appeared to influence the work reported in this paper.

Acknowledgement

The authors A.C.V and VK would like to thank IIT Hyderabad and Centre for Development of Advanced Computing (CDAC) for computational facility. A.C.V and VK acknowledges DRDO project with reference number (ERIP/ER/201701001/M/01/1711) for funding.

References

- [1] Xingxing Li, Jinlong Yang, First-principles design of spintronics materials, *Natl. Sci. Rev.* 3 (2016) 365–381.
- [2] J.K. Kawasaki, Heusler interfaces-opportunities beyond spintronics, *APL. Mater.* 7 (2019) 080907.
- [3] C. Guillemand, S. Petit-Watelot, J.C. Rojas-Sánchez, J. Hohlfeld, J. Ghanbaja, A. Bataille, P. Le Févre, F. Bertran, S. Andrieu, Polycrystalline Co₂Mn-based Heusler thin films with high spin polarization and low magnetic damping, *Appl. Phys. Lett.* 115 (2019) 172401.
- [4] X. Martí, I. Fina, D. Yi, J. Liu, J. Chu, C. Rayan-Serrao, S. Suresha, J. Zeleany, T. Jungwirth, J. Fontcuberta, R. Ramesh, *Nat. Comm.* 5 (2014) 4671.
- [5] L. Chang, M. Wang, L. Liu, S. Luo, P. Xiao, A brief introduction to giant magnetoresistance, 2014, [arXiv:1412.7691](#).
- [6] C. Giebel, D.J. Adelerhof, A.E.T. Kuiper, J.B.A. van Zon, D. Oelgeschläger, G. Schulz, *Sensors Actuators A* 91 (2001) 16–20.
- [7] S. Bhatti, S. Sbiaa, R. Hirohata, A. Ohno, H. Fukami, S. Piramanayagam, Spintronics based random access memory: a review, *Mater. Today* 20 (2017) 530–548.
- [8] T. Iwase, Y. Sakuraba, S. Bosu, K. Saito, S. Mitani, K. Takanashi, *Appl. Phys. Exp.* 2 (2009) 063003.
- [9] S.S.P. Parkin, K.P. Roche, M.G. Samant, P.M. Rice, R.B. Beyers, R.E. Scheuerlein, E.J. O'sullivan, S.L. Brown, J. Buccigano, D.W. Abraham, Yu. Lu, M. Rooks, P.I.L. Trouilloud, R.A. Wanner, W.J. Gallagher, Exchange-biased magnetic tunnel junctions and application to nonvolatile magnetic random access memory, *J. Appl. Phys.* 85 (1999) 5828.
- [10] David D. Djayaprawira, Koji Tsunekawa, Motonobu Nagai, et al., 230 Room-temperature magnetoresistance in CoFeB/MgO/CoFeB, *Appl. Phys. Lett.* 86 (2005) 092502.
- [11] D. Ralph, M. Stiles, Spin transfer torque, *J. Magn. Magn. Mater.* 320 (2008) 1190–1216.
- [12] B. Yan, C. Felser, Topological materials: Weyl semimetals, *Ann. Rev. Cond. Mat. Phys.* 8 (2017) 337–354.
- [13] J.F. Gregg, I. Petej, E. Jouguelet, C. Dennis, Spin electronics- a review, *J. Phys. D: Appl. Phys.* 35 (2002) R121–R155.
- [14] R. Yu, W. Zhang, H.J. Zhang, S.C. Zhang, X. Dai, Z. Fang, Quantized anomalous Hall effect in magnetic topological insulators, *Science* 329 (2010) 61–64.
- [15] K. Manna, Y. Sun, L. Muechler, J. Kubler, C. Felser, Heusler, Weyl, Berry, *Nat. Rev. Mater.* 3 (2018) 244–256.
- [16] Y. Tokura, K. Yasuda, A. Tsukazaki, Magnetic topological insulators, *Nat. Rev. Phys.* 1 (2019) 126–143.
- [17] C. Fu, Y. Sun, C. Felser, Topological thermoelectrics, *APL. Mater.* 8 (2020) 040913.
- [18] Y.L. Chen, J.G. Analytis, J.H. Chu, Z.K. Liu, S.K. Mo, X.L. Qi, H.J. Zhang, D.H. Lu, X. Dai, Z. Fang, S.C. Zhang, I.R. Fisher, Z. Hussain, Z.X. Shen, Experimental realization of a three-dimensional topological insulator, Bi₂Te₃, *Science* 325 (2009) 178.
- [19] D. Hsieh, Y. Xia, D. Qian, L. Wray, F. Meier, J.H. Dil, J. Osterwalder, L. Patthey, A.V. Fedorov, H. Lin, A. Bansil, D. Grauer, Y.S. Hor, R.J. Cava, M.Z. Hasan, Observation of time-reversal-protected single-Dirac-cone topological-insulator states in Bi₂Te₃ and Sb₂Te₃, *Phys. Rev. Lett.* 3 (2009) 146401.
- [20] C. Shekhar, A.K. Nayak, Y. Sun, M. Schmidt, M. Nicklas, I. Leermakers, U. Zeitler, Y. Skourski, J. Wosnitza, Z. Liu, Y. Chen, W. Schnelle, H. Borrmann, Y. Grin, C. Felser, B. Yan, Extremely large magnetoresistance and ultrahigh mobility in the topological Weyl semimetal candidate NbP, *Nat. Phys.* 11 (2015) 645–649.
- [21] M.N. Ali, J. Xiong, S. Flynn, J. Tao, Q.D. Gibson, L.M. Schoop, T. Liang, N. Haldolaarachchige, M. Hirschberger, N.P. Ong, R.J. Cava, Large, non-saturating magnetoresistance in WTe₂, *Nature* 514 (2014) 205.
- [22] E. Mun, H. Ko, G.J. Miller, G.D. Samolyuk, S.L. Bud'ko, P.C. Canfield, Magnetic field effects on transport properties of PtSn₄, *Phys. Rev. B* 85 (2012) 035135.
- [23] C. Fu, S.N. Guin, T. Scaffidi, Y. Sun, R. Saha, S.J. Watzman, A.K. Srivastava, G. Li, W. Schnelle, S.S.P. Parkin, C. Felser, J. Gooth, Largely Suppressed Magneto-Thermal Conductivity and Enhanced Magneto-Thermoelectric Properties in PtSn, *Research* (Washington, D.C., 2020, 4643507.

- [24] D.T. Son, B.Z. Spivak, Chiral anomaly and classical negative magnetoresistance of Weyl metals, *Phys. Rev. B.* 88 (2013) 104412.
- [25] X. Huang, L. Zhao, Y. Long, P. Wang, D. Chen, Z. Yang, H. Liang, M. Xue, H. Weng, Z. Fang, X. Dai, G. Chen, Observation of the chiral-anomaly-induced negative magnetoresistance in 3D Weyl semimetal TaAs, *Phys. Rev. X.* 5 (2015) 031023.
- [26] F. Heusler, Über magnetische Manganlegierungen und Verhandlungen der Deutschen, *Phys. Gese.* 5 (1903) 219.
- [27] Stanislav Chadov, Xiaoliang Qi, Jürgen Kübler, et al., Tunable multifunctional topological insulators in ternary Heusler compounds, *Nature Mater.* 9 (2010) 541–545.
- [28] L. Wollmann, A.K. Nayak, S.S.P. Parkin, C. Felser, Heusler 4.0, tunable materials, *Ann. Rev. Mater. Res.* 47 (2016) 247–270.
- [29] Koustuv Manna, Lukas Muechler, Ting-Hui Kao, et al., From Colossal to zero: Controlling the anomalous Hall effect in magnetic Heusler Compounds via berry curvature design, *Phys. Rev. X.* 8 (2018) 041045.
- [30] M. Glas, D. Ebke, I.M. Imort, P. Thomas, G. Reiss, Anomalous hall effect in perpendicularly magnetized mn_3xga thin films, *J. Magn. Magn. Mater.* 333 (2013) 134–137.
- [31] Junfeng Hu, Benedikt Ernst, Sa Tu, et al., Anomalous Hall and nernst effects in Co_2TiSn and $\text{Co}_2\text{Ti}_{0.6}\text{V}_{0.4}\text{Sn}$ Heusler thin films, *Phys. Rev. Appl.* 10 (2018) 044037.
- [32] Helena Reichlova¹, Richard Schlitz¹, Sebastian Beckert¹, et al., Large anomalous nernst effect in thin films of the Weyl semimetal Co_2MnGa , *App. Phys. Lett.* 113 (2018) 212405.
- [33] Anastasios Markou, Dominik Kriegner, Jacob Gayles, et al., Thickness dependence of the anomalous Hall effect in thin films of the topological semimetal Co_2MnGa , *Phys. Rev. B.* 100 (2019) 054422.
- [34] R.P. Dulal, B.R. Dahal, A. Forbes, I.L. Pegg, J. Philip, Large magnetization and high curie temperature in highly disordered nanoscale Fe_2CrAl thin films, *J. Magn. Magn. Mater.* 423 (2017) 314–317.
- [35] N. Nagaosa, J. Sinova, S. Onoda, A.H. MacDonald, N.P. Ong, Anomalous Hall effect, *Rev. Modern Phys.* 82 (2010) 1539–1592.
- [36] Z. Xiao, D. Yao, Y. Fang, Niu, Berry-phase effect in anomalous thermoelectric transport, *Phys. Rev. Lett.* 97 (2006) 026603.
- [37] D.J. Thouless, M. Kohmoto, M.P. Nightingale, den Nijs, Quantized Hall conductance in a two-dimensional periodic potential, *Phys. Rev. Lett.* 49 (1982) 405–408.
- [38] D. Xiao, M.C. Chang, Niu, Berry phase effects on electronic properties, *Rev. Modern Phys.* 82 (2009) 1–48.
- [39] E.M. Pugh, Rostoker, Hall effect in ferromagnetic materials, *Rev. Modern Phys.* 25 (1953) 151–157.
- [40] T. Liang, J. Lin, Q. Gibson, et al., Anomalous Hall effect in ZrTe_5 , *Nat. Phys.* 14 (2018) 451.
- [41] W. Nernst, Ueber die electromotorischen Kräfte, welche durch den Magnetismus in voneinander Wärmestrome durchflossenen Metallplatten geweckt werden, *Ann. Der Phys.* 267 (1887) 760–789.
- [42] M. Ikhlas, T. Tomita, T. Koretsune, M.-T. Suzuki, D. Nishio-Hamane, R. Arita, Y. Otani, S. Nakatsuji, Large anomalous Nernst effect at room temperature in a chiral antiferromagnet, *Nat. Phys.* 13 (2017) 1085.
- [43] J. Kerr, On rotation of the plane of polarization by reflection from the pole of a magnet, *Philos. Mag. J. Sci.* 3 (1877) 321–343.
- [44] M.H. Kim, G. Achas, M.H. Yang, et al., Determination of the infrared complex magnetoconductivity tensor in itinerant ferromagnets from Faraday and Kerr measurements, *Phys. Rev. B.* 75 (2007) 214416.
- [45] F.J. Kahn, P.S. Pershan, J. Remeika, Ultraviolet magneto-optical properties of single-crystal orthoferrites, garnets, and other ferric oxide, *Compounds* 186 (1969) 891–918.
- [46] E. Liu, Y. Sun, N. Kumar, L. Muechler, A. Sun, L. Jiao, S.Y. Yang, D. Liu, A. Liang, Q. Xu, J. Kroder, V. Süß, H. Borrman, C. Shekhar, Z. Wang, C. Xi, W. Wang, W. Schnelle, S. Wirth, Y. Chen, S.T.B. Goennenwein, C. Felser, Giant anomalous Hall effect in a ferromagnetic Kagomé-lattice semimetal, *Nat. Phys.* 14 (2018) 1125–1131.
- [47] J. Shen, Q. Zeng, S. Zhang, H. Sun, Q. Yao, X. Xi, W. Wang, G. Wu, B. Shen, Q. Liu, E. Liu, Giant anomalous Hall current driven by both intrinsic and extrinsic contributions in magnetic Weyl semimetal $\text{Co}_3\text{Sn}_2\text{S}_2$ advanced functional materials, *Adv. Funct. Mater.* 30 (2020) 2000830.
- [48] S.N. Guin, K. Manna, J. Noky, S.J. Watzman, C. Fu, N. Kumar, W. Schnelle, C. Shekhar, Y. Sun, J. Gooth, C. Felser, Anomalous Nernst effect beyond the magnetization scaling relation in the ferromagnetic Heusler compound Co_2MnGa , *NPG. Asia. Mater.* 11 (2019) 1–9.
- [49] A. Sakai, Y.P. Mizuta, A. Nugroho, R. Sihombing, T. Koretsune, M.T. Suzuki, N. Takemori, R. Ishii, D. Nishio-Hamane, R. Arita, Goswami, P. Nakatsuji, Giant anomalous nernst effect and quantum-critical scaling in a ferromagnetic semimetal, *Nat. Phys.* 14 (2018) 1119.
- [50] P.G. Van Engen, K.H.J. Buschow, R. Jongebreur, M. Erman, PtMnSb-a material with very high magneto-optical Kerr effect, *Appl. Phys. Lett.* 42 (1983) 202.
- [51] R. Carey, D.M. Newman, M.L. Wears, Giant low-temperature enhancement of magneto-optic Kerr effects in PtMnSb, *Phys. Rev. B.* 62 (2000) 1520.
- [52] G. Kresse, D. Joubert, From ultrasoft pseudopotentials to the projector augmented-wave method, *Phys. Rev. B.* 59 (1999) 1758.
- [53] G. Kresse, J. Furthmüller, Efficient iterative schemes for ab initio total-energy calculations using a plane-wave basis set, *Phys. Rev. B.* 54 (1996) 11169.
- [54] J.P. Perdew, K. Burke, M. Ernzerhof, Generalized gradient approximation made simple, *Phys. Rev. Lett.* 77 (1996) 3865.
- [55] H. Ebert, D. Ködderitzsch, J. Minár, Calculating condensed matter properties using the KKR-green's function method-recent developments and applications, *Rep. Progr. Phys.* 74 (2011) 096501.
- [56] Nicola Marzari, David Vanderbilt, Maximally localized generalized Wannier functions for composite energy bands, *Phys. Rev. B.* 56 (1997) 12847.
- [57] Nicola Marzari, Arash A. Mostofi, Jonathan R. Yates, Ivo Souza, David Vanderbilt, Maximally localized Wannier functions: Theory and applications, *Rev. Modern Phys.* 84 (2012) 1419.
- [58] A.A. Mostofi, J.R. Yates, Y.S. Lee, I. Souza, D. Vanderbilt, N. Marzari, Wannier90: A tool for obtaining maximally-localised Wannier functions, *Comput. Phys. Comm.* 178 (2008) 685–699.
- [59] J.E. Avron, Osadchy, D., Seiler, A topological look at the quantum hall effect, *Phys. Today* 56 (2003) 38.
- [60] Q. Wu, S. Zhang, H.F. Song, M. Troyer, Soluyanov, Wanniertools: An open-source software package for novel topological materials, *Comput. Phys. Comm.* 224 (2018) 405–416.
- [61] X. Wang, J.R. Yates, I. Souza, D. Vanderbilt, Ab-initio calculation of the anomalous Hall conductivity by Wannier interpolation, *Phys. Rev. B.* 4 (2006) 195118.
- [62] Y. Yao, L. Kleinman, A.H. MacDonald, J. Sinova, T. Jungwirth, D.S. Wang, E. Wang, Q. Niu, First-principles calculation of anomalous Hall conductivity in ferromagnetic bcc Fe, *Phys. Rev. Lett.* 92 (2004) 037204.
- [63] I. Galanakis, P.H. Dederichs, N. Papanikolaou, Slater-Pauling behavior and origin of the half-metallicity of the full-Heusler alloys, *Phys. Rev. B.* 66 (2002) 174429.
- [64] Bing Lv, Zhongyuan Lian, Yu Miao, Cunxu Gao, Mingsu Si, Desheng Xue, Fucheng Yu, Jinli Yao, Realization of a Heusler alloy Mn_2FeAl with B2 ordering, *Appl. Phys. Lett.* 116 (2020) 132404.
- [65] R. Mohankumar, S. Ramasubramanian, M. Rajagopalan, M. Manivel Raja, S.V. Kamat, J. Kumar, Density functional study of half-metallic property on B2 disordered Co_2FeSi , *J. Mater. Sci.* 50 (2015) 1287–1294.
- [66] Hasnip Philip James, C.H. Loach, J.H. Smith, Probert Matthew Ian James, Gilks Daniel, Sizeland James, Yoshida Kenta, Oogane Mikihiko, Hirohata Atsufumi, Lazarov Vlado, B2 atomic disorder in $\text{Co}_2\text{Fe}_x\text{Mn}_{1-x}\text{Si}$ Heusler alloys, *J. Magn. Soc. Jpn.* 38 (2014) 50–55.
- [67] K. Seema, N.M. Umran, Ranjan Kumar, Effect of disorder on electronic, magnetic, and optical properties of Co_2CrZ Heusler alloys ($Z = \text{Al}, \text{Ga}, \text{Si}, \text{Ge}$), *J. Supercond. Nov. Magn.* 29 (2016) 401–408.
- [68] P. Bruski, S.C. Erwin, M. Ramsteiner, O. Brandt, K.-J. Friedland, R. Farshchi, J. Herfort, H. Riechert, Disorder-induced reversal of spin polarization in the Heusler alloy Co_2FeSi , *Phys. Rev. B* 83 (2011) 140409.
- [69] P.G. Van Engen, K.H.J. Buschow, Magneto-optical properties of metallic ferromagnetic materials, *J. Magn. Magn. Mater.* 30 (1983) 374.
- [70] K.H. Buschow, P.G. van Engen, Magnetic and magneto-optical properties of heusler alloys based on aluminium and gallium, *J. Magn. Magn. Mater.* 25 (1981) 90–96.
- [71] R. Silva, Rajendra Saxena, Jacob Schaf, F. Livi, Zawislak, Magnetic hyperfine field on Ta in the Co_2HfAl and Co_2HfGa Heusler alloys, *Hyp. Inter.* 9 (1981) 489–493.
- [72] B.A. Salma, G. Gao, K. Yao, Half-metallicity and magnetism of Heusler alloys Co_2HzZ ($Z=\text{Al}, \text{Ga}, \text{Ge}, \text{Sn}$), *J. Magn. Magn. Mater.* 441 (2017) 356.
- [73] M. Yin, S. Chen, P. Nash, Enthalpies of formation of selected Co_2YZ Heusler compounds, *J. Alloys. Comp.* 577 (2013) 49–56.
- [74] A. Liechtenstein, M. Katsnelson, V. Antropov, V. Kubanov, Local spin density functional approach to the theory of exchange interactions in ferromagnetic metals and alloys, *J. Magn. Magn. Mater.* 67 (1987) 65.
- [75] P.W. Anderson, Theory of magnetic exchange interactions: Exchange in insulators and semiconductors, *Solid. State. Phys.* 14 (1963) 99.
- [76] Wei, Xiao-Ping, Exchange interactions and curie temperatures in Fe_2NiZ compounds, *J. Alloys. Comp.* 694 (2017) 1254.
- [77] J. Rusz, I. Turek, M. Diviš, Random-phase approximation for critical temperatures of collinear magnets with multiple sublattices:GdX compounds ($x = \text{Mg}, \text{Rh}, \text{Ni}, \text{Pd}$), *Phys. Rev. B* 71 (2005) 174408.
- [78] R. Logemann, A.N. Rudenko, M.I. Katsnelson, A. Kirilyuk, Exchange interactions in transition metal oxides: the role of oxygen spin polarization, *J. Phys.: Condens. Matter* 29 (2017) 335801.
- [79] Charles S. Spencer, Jacob Gayles, Nicholas A. Porter, et al., Helical magnetic structure and the anomalous and topological Hall effects in epitaxial films, *Phys. Rev. B.* 97 (2018) 214406.
- [80] E.I. Kondorskii, *Zh. Eksp. Teor. Fiz.* 55 (1968) 558.
- [81] P. Rambabu, C.V. Anusree, M. Manivel Raja, V. Kanchana, Anomalous Hall and Nernst conductivities in Co_2NbGa : A first principles study, *J. Magn. Magn. Mater.* 538 (2021) 168303.
- [82] J. Noky, Y. Zhang, J. Gooth, et al., Giant anomalous Hall and Nernst effect in magnetic cubic Heusler compounds, *Npj. Comput. Mater.* 6 (2020) 77.
- [83] Y. Sakuraba, K. Hyodo, A. Sakuma, et al., Giant anomalous Nernst effect in the $\text{Co}_2\text{MnAl}_1-x\text{Si}_x$ Heusler alloy induced by Fermi level tuning and atomic ordering, *Phys. Rev. B.* 101 (2020) 134407.

- [84] P. Weinberger, John Kerr and his effects found in 1877 and 1878, *Philo. Mag.* 88 (2008) 897–907.
- [85] F. Matthes, A. Rzhevskii, L.N. Tong, L. Malkinski, Z. Celinski, C.M. Schneider, J. *Appl. Phys.* 93 (2003) 6504.
- [86] G. Meyer, T. Crecelius, A. Bauer, I. Mauch, G. Kaindl, In situ near-field imaging of magnetic domain patterns in ultrathin iron films, *Appl. Phys. Lett.* 83 (2003) 1394.
- [87] V.I. Gavrilenko, R.Q. Wu, J. *Mag. Magn. Mat.* 260 (2003) 330.
- [88] R.P. Cowburn, Probing antiferromagnetic coupling between nanomagnets, *Phys. Rev. B.* 65 (2002) 092409.
- [89] J.P. Jamet, J. Ferre, P. Meyer, J. Gierak, C. Vieu, F. Rousseaux, C. Chappert, V. Mather, Giant enhancement of the domain Wall velocity in irradiated ultrathin magnetic nanowires, *IEEE. Trans. Magn.* 37 (2001) 2120.
- [90] M.R. Freeman, W.K. Hiebert, *Stroboscopic Microscopy of Magnetic Dynamics*, Springer, Berlin, 2002, p. 93.
- [91] H. Ebert, Magneto-optical effects in transition metal systems, *Rep. Progr. Phys.* 59 (1996) 1665.
- [92] P.M. Oppeneer, T. Maurer, J. Sticht, J. Kübler, Ab initio calculated magneto-optical Kerr effect of ferromagnetic metals: Fe and Ni, *Phys. Rev. B.* 45 (1992) 10924.